ACSNANO
www.acsnano.org
ARTICLE

# Optical Asymmetry and Nonlinear Light Scattering from Colloidal Gold Nanorods

Miao-Bin Lien,[†] Ji-Young Kim,[‡] Myung-Geun Han,[§] You-Chia Chang,[∥] Yu-Chung Chang,[⊥] Heather J. Ferguson,[†] Yimei Zhu,[§] Andrew A. Herzing,[#] John C. Schotland,[▼] Nicholas A. Kotov,[‡] and Theodore B. Norris*[,†]

[†]Department of Electrical Engineering, University of Michigan, Ann Arbor, Michigan 48109, United States
[‡]Department of Materials Science and Engineering, University of Michigan, Ann Arbor, Michigan 48109, United States
[§]Condensed Matter Physics and Materials Sciences Department, Brookhaven National Laboratory, Upton, New York 11973, United States
[∥]Department of Physics, University of Michigan, Ann Arbor, Michigan 48109, United States
[⊥]Department of Electrical Engineering, National Changhua University of Education, Changhua City 500, Taiwan
[#]National Institute of Standards and Technology, Gaithersburg, Maryland 20899, United States
[▼]Department of Mathematics, University of Michigan, Ann Arbor, Michigan 48109, United States

**ABSTRACT:** **A systematic study is presented of the intensity-dependent nonlinear light scattering spectra of gold nanorods under resonant excitation of the longitudinal surface plasmon resonance (SPR). The spectra exhibit features due to coherent second and third harmonic generation as well as a broadband feature that has been previously attributed to multiphoton photoluminescence arising primarily from interband optical transitions in the gold. A detailed study of the spectral dependence of the scaling of the scattered light with excitation intensity shows unexpected scaling behavior of the coherent signals, which is quantitatively accounted for by optically induced damping of the SPR mode through a Fermi liquid model of the electronic scattering. The broadband feature is shown to arise not from luminescence, but from scattering of the second-order longitudinal SPR mode with the electron gas, where efficient excitation of the second order mode arises from an optical asymmetry of the nanorod. The electronic-temperature-dependent plasmon damping and the Fermi−Dirac distribution together determine the intensity dependence of the broadband emission, and the structure-dependent absorption spectrum determines the spectral shape through the fluctuation−dissipation theorem. Hence a complete self-consistent picture of both coherent and incoherent light scattering is obtained with a single set of physical parameters.**

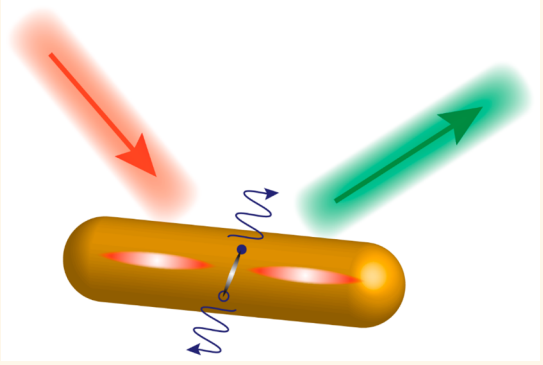

**KEYWORDS:** *plasmonics, nonlinear optics, nanophotonics, condensed matter science, gold nanorods*

Nanoscale noble metal structures, such as gold and silver nanoparticles, exhibit optical and electronic properties that are not observed in their bulk counterparts. The electromagnetic modes of these systems, known as surface plasmon resonances (SPRs), lead to strong interaction with light, and an enhancement of the optical field enabling nonlinear effects to be observed with low incident light intensity.[1,2] The plasmon resonances and the field enhancement can be tailored through the choice of metal, the specific size and shape, the dielectric environment, and their mutual spatial arrangement.[3−5] In fact, the sensitivity of the resonances to the local dielectric and charge environment enables the SPR to serve as an optical interrogation of the environment and thus as an optical sensor. The attachment of chemical ligands enables selective sensing of chemical or biomedical targets. As a result, metal nanoparticles serve as important building blocks in the fields of modern chemical engineering,[6] biosensors,[7] and advanced microscopy.[8−10] A fundamental understanding of the nonlinear optical response of metal nanostructures is thus essential for the development of optical applications of plasmonics.

The two principal nonlinear optical responses that can be observed on direct far-field excitation are multiphoton luminescence (PL) and harmonic generation (HG). Both

Received: March 8, 2017
Accepted: May 16, 2017
Published: May 16, 2017

Downloaded via NATL INST OF STANDARDS & TECHNOLOGY on October 28, 2022 at 12:47:44 (UTC).
See https://pubs.acs.org/sharingguidelines for options on how to legitimately share published articles.


© 2017 American Chemical Society

DOI: 10.1021/acsnano.7b01665
ACS Nano 2017, 11, 5925−5932

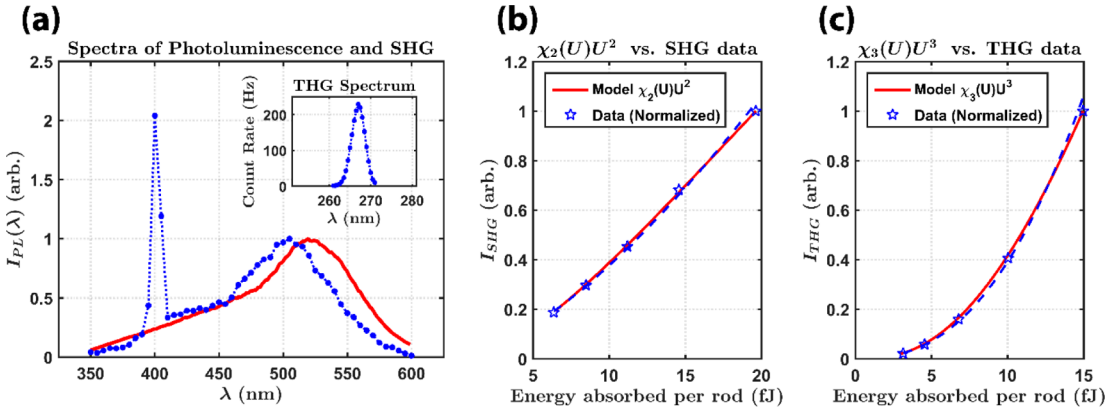


**Figure 1. Nonlinear optical response on resonant excitation with 800 nm, 50 fs ultrashort pulses (a) the spectral components include SHG, THG (inset), and a broadband PL. The red curve is the calculated spectrum with the proposed model (b) the unconventional intensity scaling of SHG (with the background PL subtracted) and (c) THG (background free). The blue dashed lines are the exponential fittings of the data and the red curves are the calculated SHG and THG with optically induced damping of the longitudinal SPR model. Notice the red curves fit the data better than the exponential fitting.**

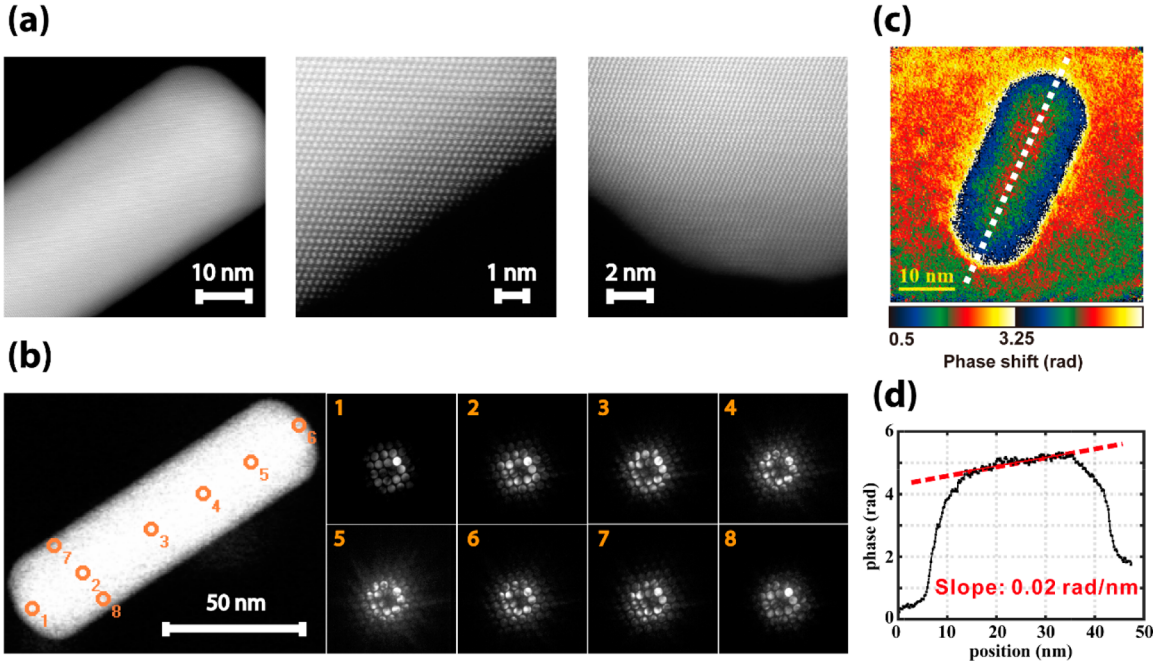


**Figure 2. (a) Atomic-resolution high-angle annular dark-field (HAADF) images of a single AuNR used in the optical experiment and (b) convergent beam electron diffraction (CBED) pattern collected with beam positioned at various locations (orange markers) in the AuNR. Results indicated consistent structure in all areas of the rod and showed the high degree of structural symmetry of the AuNRs. (c) False-color reconstructed phase shift image and (d) its line profile along the long axis (white dashed line in d) of the AuNR.**

phenomena have been investigated extensively. Early observations of two-photon luminescence (TPL) were reported by Boyd et al.,[11] and interpreted as the generation and recombination of electron−hole pairs involving the d-band and the conduction (sp) band. The luminescence efficiency of gold nanoparticles can be remarkably high,[12] suggesting applications to biological labeling and imaging.[13] More recently, harmonic generation from metal nanoparticles has received considerable attention. Lippitz et al. reported the first observation of third-harmonic generation (THG) from individual gold colloidal particles down to 40 nm diameter,[14] and third harmonic imaging experiments with gold nanorods was demonstrated;[15] SHG from gold nanorods was also investigated in ref 16. A phenomenological theory of second harmonic generation (SHG) from centrosymmetric spherical metallic particles was developed by J. I. Dadap et al.[17,18] Starting with the second order nonlinear surface susceptibilities, they presented a general electro-magnetic theory of SH Rayleigh scattering (SHRS) for spheres within the small particle limit, including the contribution from the bulk nonlinear response compatible with isotropic symmetry. They predicted a quadrupolar-type radiation pattern, as the second order process is in principle dipole-forbidden in centrosymmetric material with centrosymmetric geometry, consistent with experimental results on hyper-Rayleigh scattering from silver nanospheres reported by Hao et al.[19] and a series of polarization analysis experiments performed by Brevet et al.[20−22]

On optical excitation with ultrashort optical pulses, gold nanorods (AuNRs) exhibit hyper-Rayleigh scattering (SHG and



DOI: 10.1021/acsnano.7b01665
ACS Nano 2017, 11, 5925−5932

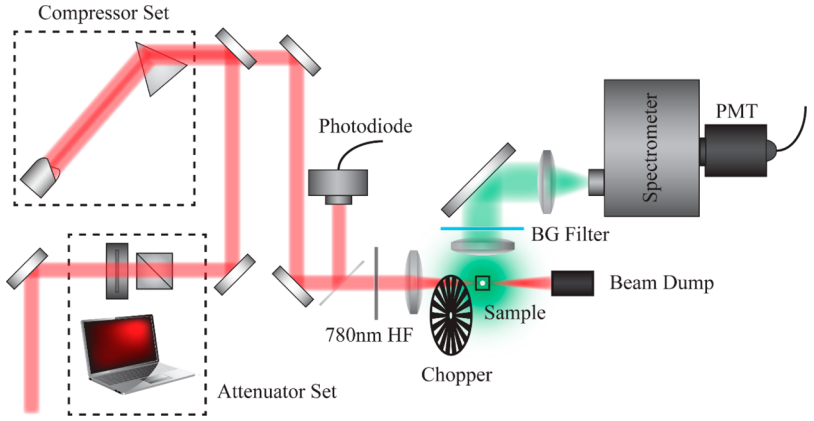


**Figure 3. Experimental setup for the spectral and intensity dependence study on the nonlinear light scattering from AuNRs.**

THG) as well as a broadband feature attributed to PL. An example of the scattered light spectrum under 800 nm 50 fs excitation in our experiments (discussed in detail below) displays these features as shown in Figure 1a. These responses have been respectively interpreted in terms of conventional nonlinear optical processes[15,23] and multiphoton interband luminescence processes.[12,24−26] There are, however, features of the data whose interpretation is problematic with these physical models. The SHG signal, for example, is surprisingly strong, whereas in contrast to the prediction that, in the small particle limit, SHG should be forbidden given the assumed centrosymmetry of the system; the observed SHG has rather been attributed to the effects of either the metal-media interface or retardation.[17−22] Additionally, the SHG and THG signals from AuNRs show saturation-like characteristics in the power scaling (see Figure 1b,c), which have been either overlooked due the contribution from the background PL[23] or ambiguously attributed to damage of the nanoparticles.[15] The broadband spectral feature that has been attributed to PL in gold nanoantennas has recently been shown to depend primarily on the nanoscale geometry, and does not in fact arise from the electronic band structure.[27] Finally, the nonlinear response has been theoretically predicted to exhibit unusual scaling with excitation intensity due to surface confinement effects on the electrons undergoing collective oscillation in the SPR.[28]

Among the most common forms of structure used for studies of nanoplasmonics are chemically synthesized AuNRs, grown in aqueous solution guided by the surfactant cetyltrimethylammonium bromide (CTAB).[29] These structures exhibit a high degree of structural symmetry and crystallinity, as can be seen from the atomic-resolution high-angle annular dark-field images and convergent beam electron diffraction pattern of a single AuNR of the sample used in these experiments in Figure 2a,b. A spatial analysis of the electrostatic potential around AuNRs was recently performed using off-axis electron holography.[30] In the absence of magnetic field, the phase shift $\phi(x, y)$ in an electron wave after passing through a specimen is proportional to a line integral of the electrostatic potential along the propagation direction.[31] The reconstructed phase shift $\phi(x, y)$ map obtained for a AuNR shows a considerable asymmetry and a distinctive slope along the long axis of the rod as seen in Figure 2c,d, indicating the presence of a static dipole moment. In a recent companion study,[32] we have found that nonuniform coverage of the surfactant CTAB induces a static dipole moment, which breaks the inversion symmetry and leads to an optical asymmetry. This has far-reaching consequences, since for an optically symmetric nanoparticle, SHG is forbidden to lowest order, and can arise only through the effect of retardation and quadrupole radiation. We show in this article that the optical symmetry breaking by the static dipole in AuNRs enables a quantitative and self-consistent explanation of all the major features of nonlinear light scattering.

## RESULTS AND DISCUSSION

Figure 1a displays a typical light scattering spectrum from a dilute colloidal AuNR sample under excitation from ultrashort laser pulses at 800 nm; the spectra exhibit resonant features at the second and third harmonic wavelengths, as well as a broadband component. We present here the experimental details and physical model that can simultaneously, self-consistently, and quantitatively explain these features.

The experimental setup is shown in Figure 3. The excitation source is a Ti:sapphire mode-locked laser, which provides 800 nm, 50 fs pulses at a repetition rate of 76 MHz. The excitation power is controlled by a variable attenuator consisting of a half-wave plate mounted on a programmable rotator and a Glan-Thompson polarizer. The laser pulses pass through a prism compressor so that the pulses are transform-limited at the focal point. A small fraction of the beam is sampled by a photodiode in order to measure the incident power and its fluctuations. In addition, a 780 nm high-pass filter is placed before the focusing lens to ensure there is no residual SHG or THG in the excitation beam. The beam is focused in the center of a cuvette containing an aqueous solution of AuNRs with a longitudinal plasmon resonance at 808 nm. Light scattered at 90° from the excitation direction is collected by an $f^{/\#}$=1 uv-coated lens and filtered through either BG filters (BG-39, BG-40 color filters) or 267 nm band-pass filters to remove the linear 800 nm scattering. The collected signal is focused on the entrance slit of a monochromator and detected by a single photon counting photomultiplier. A chopper is placed in the excitation beam path to modulate the excitation beam in order to subtract background dark counts from the signal in gated photon counting mode.

A typical spectrum of the nonlinearly scattered light is shown in Figure 1a, showing clearly three main components: THG and SHG peaks (hyper-Rayleigh scattering) located at 267 and 400 nm, respectively, and a broadband feature ranging from 350 to 600 nm that is generally referred to as PL. We note that the SHG peak overlaps with the broadband photoluminescence. A key experiment to revealing the physical processes underlying the light scattering is the scaling of the various



DOI: 10.1021/acsnano.7b01665
ACS Nano 2017, 11, 5925−5932

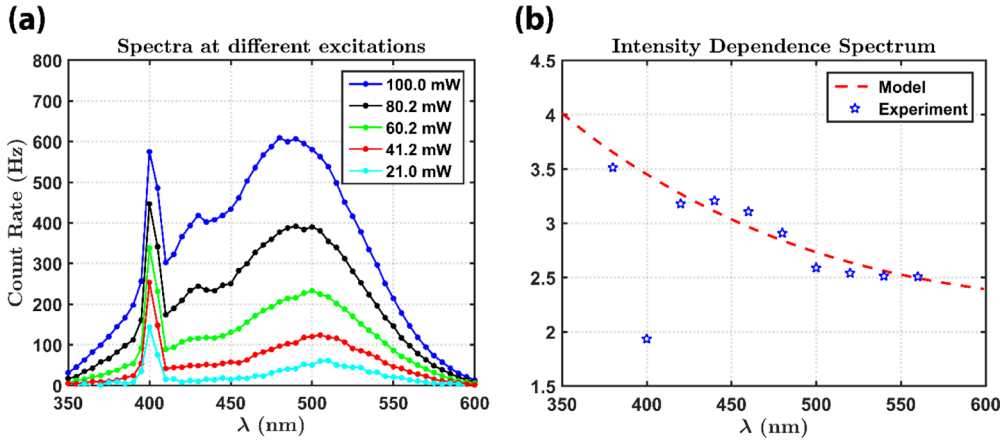


**Figure 4. (a) The spectra of nonlinear optical responses measured at different excitation intensities. (b) The spectrally resolved intensity dependent scaling. Notice the scaling at 400 nm is close to 2. The red dash curve is generated from the proposed model.**

spectral components with excitation intensity (or fluence in the case of fixed pulse duration). Figure 1b,c shows the measured scaling of the SHG and THG peaks. On the basis of the standard perturbation theory of nonlinear optics,[33] the SHG should scale exactly as the square of the intensity, and the THG as the cube.

The THG signal has a well-defined spectral peak at 267 nm and is background-free (Figure 1 inset). A fit to a scaling curve of the form $I_{sig} = a(I_{ex})^b$ yields an exponent of 2.46 (±0.022), quite different from the expected value of 3. The SHG peak at 400 nm sits on top of the broad PL background. To determine the SHG scaling, we subtract the PL before integrating the area under the 400 nm peak (the assumption that the PL spectrum is smooth is fully justified by the model below). The background-subtracted SHG scales with an exponent of 1.49 ± 0.03, far from its conventional expected value of 2.

Nonlinear optical processes are often described using an expansion of the nonlinear susceptibility in powers of the optical field.[33] In the strict limits of $\chi^{(2)}$ and $\chi^{(3)}$, the SHG and THG signals must respectively scale quadratically and cubically with the intensity. The unexpected scaling of the SHG and THG signals at even the lowest fluence can be seen as a breakdown of this approximation. Nevertheless, the experimental scaling can be explained quantitatively within this framework by optically induced damping of the longitudinal SPR by hot electrons.[34,35] In a model of the SPR mode of the AuNR as a classical anharmonic oscillator, the second and third order nonlinear susceptibilities $\chi^{(2)}$ and $\chi^{(3)}$ are related to the linear susceptibility $\chi^{(1)}$ by

$$\chi^{(2)}(\omega) \propto \chi^{(1)}(2\omega)[\chi^{(1)}(\omega)]^2 \text{ and } \chi^{(3)}(\omega) \propto \chi^{(1)}(3\omega)[\chi^{(1)}(\omega)]^3$$

where

$$\chi^{(1)}(\omega) = \frac{N(e^2/m)}{\epsilon_0 D(\omega)},\ D(\omega) = \omega_0^2 - \omega^2 - 2i\omega\gamma$$

and $\omega_0$ is the material resonance frequency.

The factor $D(\omega)$ contains the resonance frequency of the system (corresponding to 808 nm wavelength for the longitudinal plasmon mode of the AuNR) and the damping rate $\gamma$. It has been shown that scattering of the nanoparticle plasmon from single-particle excitations of the electron gas is the dominant nonlinearity in the optical response, as $\gamma$ depends on the electron temperature.[35] Following the Fermi liquid model of ref 35, we find the intensity scaling will be modified by the pump-induced electron heating according to

$$I_{SHG} \propto \chi^{(2)}(\omega)I^2 \propto [I/\gamma_p]^2 \text{ and } I_{THG} \propto \chi^{(3)}(\omega)I^3 \propto [I/\gamma_p]^3$$

where

$$\gamma_p \propto \gamma_{ee} = \frac{\int_0^\infty f(\varepsilon)\gamma_{ee}(\varepsilon)d\varepsilon}{\int_0^\infty f(\varepsilon)d\varepsilon}$$

is the total electron-temperature-dependent scattering rate and

$$\gamma_{ee}(\varepsilon, T_e) = \gamma_0 + \frac{K(\pi k_B T_e)^2 + (\varepsilon - \varepsilon_F)^2}{1 + \exp[-(\varepsilon - \varepsilon_F)/k_B T_e]}$$

The model has only two fitting parameters, namely $\gamma_0$, the electronic-temperature-independent part of $\gamma_{ee}$, and $U_{abs}$, the absorbed pulse energy per AuNR that results in heating the conduction band electrons.[36] The SHG and THG scaling fit the model very well (data fits are 1.49, 2.46 and the model predictions are 1.47, 2.41 for SHG and THG, respectively) for a single value of $\gamma_0 = 0.067$ (fs$^{-1}$) and $U_{abs} \approx 0.267U_{th}$, where $U_{th}$ is the absorbed energy estimated from the estimated incident intensity and a classical model of the absorption cross section of a AuNR.[4] In fact, it can be seen in Figure 1c,d that the Fermi liquid model fits the scaling data better than an assumed power law scaling. We conclude that the SPR damping induced by a hot thermal distribution of single-particle excitations quantitatively accounts for the unexpected scaling of the nonlinear optical response of the AuNR longitudinal plasmon resonance.

We now discuss the broadband scattered light, which has generally been attributed to PL arising from the recombination of d-band holes with conduction band electrons excited by multiphoton absorption in prior work. Our key experiment is the measurement of the complete spectral dependence of the intensity scaling of the broadband emission, as shown in Figure 4b. The scattered light scales with an exponent of approximately 3.6 at 375 nm to 2.5 above 550 nm; i.e., the shorter wavelength emission exhibits a more highly nonlinear behavior. Interestingly, the total signal at 400 nm (i.e., the sum of the coherent SHG and the broadband signal) does not follow the general trend, but scales with an exponent of 1.92. While multiphoton PL from interband transitions can account for some features of the spectrum,[8,12,37] others are inconsistent with PL as the source of the broadband emission. In particular,


DOI: 10.1021/acsnano.7b01665
ACS Nano 2017, 11, 5925−5932

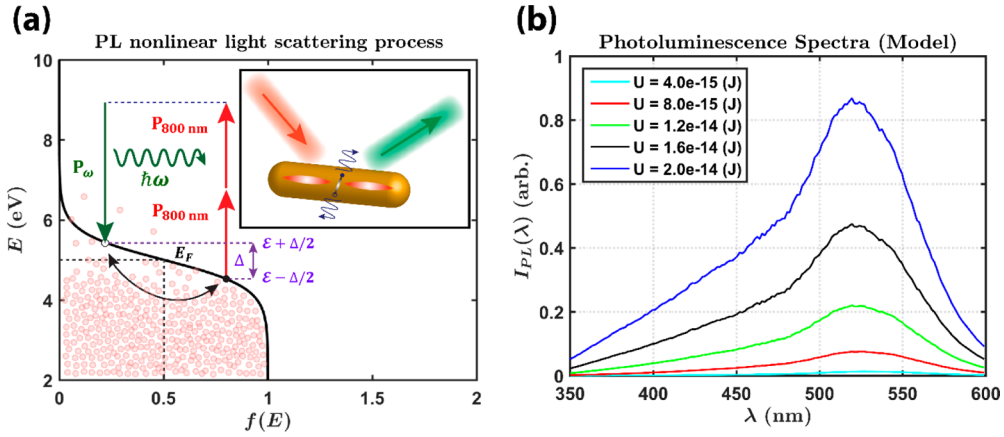


**Figure 5. (a) Energy diagram of the PL nonlinear light scattering process and (inset) a physical illustration of the 2nd order plasmon excitation and the PL generation. (b) Calculated scattered light spectrum using the values of $\gamma_{ee}$ and $U_{abs}$ obtained from the SHG and THG experiments. The spectral line shape is determined by the (structure dependent) absorption spectrum of AuNRs, i.e., the measured UV−vis spectrum.**

the spectral features of the broadband spectrum from AuNRs do not really match well with those from their bulk counterpart, though some previous work has attempted to attribute these features to recombination processes between conduction band electrons and d-band holes near the X and L symmetry points in the Brillouin zone.[8,24−26] Recent experiments comparing PL from gold nanoantennas fabricated from single crystals and polycrystalline films, however, have suggested that it is the nanoscale geometry of the plasmonic structures that determines the shape of the emission spectra,[27] and not the band structure. Other recent work on PL from plasmonic metals also suggests that scattering from electronic excitations rather than traditional luminescence is responsible for light emission.[38] We therefore performed an additional set of experiments in which the AuNRs were excited directly with 400 nm 50 fs pulses (generated by frequency doubling the Ti:sapphire laser), which should induce one-photon absorption energetically equivalent to 2-photon absorption at 800 nm. The threshold for absorption from the d bands in Au is 1.8 eV; hence 800 nm excitation from the d-band requires two- or three-photon absorption, while linear absorption of 400 nm light can excite d-band holes. We found there was only negligible emission from the AuNRs under 400 nm excitation even at the highest accessible excitation intensity; this indicates unequivocally that the broadband emission under 800 nm excitation does not arise from interband transitions as is usually thought.

Given that the broadband emission is not in fact interband PL, we propose a model in which the nonlinear light scattering arises from an interplay of the plasmon damping and the optical anisotropy due to the presence of a static dipole on the AuNRs. On illumination with 800 nm pulses, the gold nanorod's longitudinal plasmon mode, corresponding to a collective oscillation of the electrons along the long axis of the particle, is resonantly excited. The charge asymmetry associated with the static dipole along the nanorod axis gives rise to a nonzero $\chi^{(2)}$; the second-order nonlinear polarization along the nanorod axis excites the asymmetric second-order longitudinal plasmon mode, which can efficiently scatter with the background free electron gas just as the fundamental plasmon mode scatters, as described above.

The process is illustrated in Figure 5a, indicating how two longitudinal plasmons excited by the pump give rise to a fluctuating polarization $P_\omega$ due to scattering from the free electron gas. Electrons oscillating in opposite directions in the asymmetric second-order longitudinal mode scatter with free carriers, producing dipole fluctuations along the transverse nanorod axis, see Figure 5a inset. The emission arises as radiation from $P_\omega$, and the coupling of these dipole fluctuations to free-space electromagnetic modes is enhanced by the transverse plasmon mode of the AuNRs. As illustrated in Figure 5a, a continuum of radiation is produced since the scattering of an electron with initial energy $\varepsilon - \Delta/2$ to a final state with energy $\varepsilon + \Delta/2$ results in a shift $\Delta$ of the emission relative to the second harmonic of the 800 nm excitation; the broadband spectrum arises from an integral over all possible initial and final free-carrier states with occupations $f_i$ and $f_f$ determined by the Fermi function for a carrier gas with electron temperature $T_e$, which is well-known from the scaling experiments on SHG and THG discussed above. Since the nonlinear light scattering is driven by scattering of plasmons from free carriers, the total emission should be proportional to the plasmonic damping rate, $\gamma_p \propto \gamma_{ee}$. Finally, the spectrum of scattered light is generally determined by the Fourier transform of the dipole−dipole correlation function.[39] By the fluctuation−dissipation theorem, this correlation function is proportional to the imaginary part of the susceptibility, i.e., the absorption spectrum.[39−41] Physically, the scattering-induced fluctuations in the polarization radiate with a strength proportional to the absorption spectrum. This effect is included by incorporating a line shape factor $L(\omega)$ which is obtained from the actual experimental absorption spectrum of the AuNR sample. Putting all these elements together, the broadband scattered light will be given by the expression

$$I(\lambda, U) = I(\omega, T_e) \propto \int f(\varepsilon - \Delta/2)[1 - f(\varepsilon + \Delta/2)]d\varepsilon \cdot \gamma_{ee}(T_e) \cdot L(\omega)$$

where

$$\Delta = 2\hbar\omega_{800\text{nm}} - \hbar\omega \text{ and } f(\varepsilon) = \frac{1}{1 + \exp\frac{(\varepsilon - \varepsilon_F)}{k_B T_e}}$$

is the Fermi function with electron temperature $T_e(U)$.

Figure 5b shows the calculated scattered light spectrum using the values of $\gamma_{ee}$ and $U_{abs}$ obtained from the SHG and THG experiments; Figure 1a shows the close match of the theory (red line) and experimental (blue dots) line shapes. Note that



DOI: 10.1021/acsnano.7b01665
ACS Nano 2017, 11, 5925−5932

the spectral smoothness around the SHG position justifies the interpolation and subtraction of the background from the SHG peak around 400 nm discussed above. Most critically, we can also generate from the calculation the intensity scaling as a function of wavelength; the result shown as the red curve in Figure 4b, and shows excellent agreement with the data. This is a strong confirmation of the model, indicating that interband PL processes do not play a significant role in the multiphoton broadband emission, but that second-order nonlinear light scattering mediated by damping of the second-order longitudinal plasmon resonance is mainly responsible for the scattered light. It should be noted the only fitting parameter in the calculation is the value of the Fermi level; the fitting leads to $\varepsilon_F$ = 5.4 (eV), which is very close to the bulk value of 5.5 (eV), and the slight difference may be due to pump-induced heating. A final confirmation that the second-order light scattering mechanism described above is correct is the observation that excitation at 400 nm only leads to negligible broadband emission; excitation at 400 nm does not induce an excitation of the second order plasmon mode which could then scatter into a fluctuating dipole transverse to the nanorod.

## CONCLUSION

In summary, we have systematically investigated nonlinear light scattering from AuNRs under resonant excitation of the longitudinal plasmon mode, with detailed measurements of the spectral dependence of the intensity scaling across the SHG, THG, and broadband components. From our recent electron holography study (reported elsewhere), we know that the structurally symmetric gold nanorods are in fact electrically and optically anisotropic due to asymmetric charge distributions induced by the ligands used to guide their self-assembly. This optical asymmetry leads to strong second-order polarizability $\chi^{(2)}$ and hence the significant SHG signal. The SHG and THG nonlinear susceptibilities are intensity dependent, through the optically induced damping of the SPR linear susceptibility, corresponding to scattering of the plasmon with hot electrons; this damping is quantitatively understood through the electron temperature dependence in the Fermi liquid model. Because of the nonzero $\chi^{(2)}$, the second-order longitudinal mode is excited. Scattering of this mode from the electron gas results in a fluctuating polarization along the transverse direction of the nanorod, which radiates a broadband spectrum. The spectrum as well as the intensity scaling are understood through a self-consistent model of light scattering. Interband transition processes apparently play no significant role in the light emission. We note finally that the model incorporates the actual SPR spectrum through the fluctuation–dissipation theorem and assumes scattering from a perfectly thermalized electron gas, and hence does not account for the individual microscopic scattering processes responsible for the radiation. It thus cannot account for the possible role of coherence in the scattering process, which may be important for the complete interpretation of the emission around 400 nm; the nearly quadratic scaling of the total signal at 400 nm (SHG + broadband component) is highly suggestive, and remains the subject for additional study.

## METHODS

**GNR Sample and the Damage Testing.** The data presented in this article are from samples consisting of aqueous solutions of AuNRs purchased from Nanopartz. The solution concentration is approximately 1 nM, sufficiently low that particle interaction effects are negligible. The AuNRs have diameter 25 nm and an average length 102 nm, leading to a transverse plasmon resonance at 517 nm and longitudinal plasmon resonance at 808 nm. The longitudinal plasmon resonance is typically inhomogeneously broadened due to residual fluctuations in the nanorod length, but it should be noted that the excitation light only interacts with nanorods having plasmon resonances close to the excitation wavelength; this was verified by control experiments showing that the signals disappeared when using samples with longitudinal plasmon energies away from resonance. The solution sample is placed in a UV transparent cuvette during the optical excitation to avoid the absorption of the scattered nonlinear optical signal.

Structural characterization of nanoparticles was carried out using scanning transmission electron microscopy (STEM). High-angle annular dark-field (HAADF) images using a primary electron beam energy of 300 keV. In addition, convergent beam electron diffraction (CBED) patterns were collected at various positions within the nanorods using a convergence angle of approximately 3.5 mrads.

In the optical experiments, we ruled out the possibility of rod melting by monitoring the difference between the initial and final UV–vis spectra of the gold nanorod solution sample. Gold nanorods in solution can be melted into spherical nanoparticles by excitation with intense femtosecond laser pulses of sufficient energy. If the energy absorbed by the rods are strong enough such that the rods are partially melted before diffusing out of the focal volume, the longitudinal absorption band would blue-shift, as the aspect ratio of the rods would decrease. If the absorbed energy is even larger such that the rods completely melt into spheres before diffusing out of the focal volume, the intensity of the longitudinal absorption band would decrease, while the intensity of the transverse absorption band would increase, suggesting the depletion of the gold nanorods and the formation of spherical nanoparticles. This phenomenon has previously been observed and reported as a valid method to monitor the rod shape change.[42] Indeed, even with the most intense excitation in our experiment, no blue-shift or the decrement of the longitudinal absorption intensity in the final UV–vis spectrum was observed, indicating that no rod melting occurred.

**Intensity Dependence Measurement.** The measurement of the intensity scaling corresponds to the determination of $\gamma$ from $y = ax^{\gamma}$ where $y$ represents the optical signal and $x$ represents the excitation intensity. The task is essentially the extraction of the fitted linear slope from the data points in a log–log plot, which must be performed in such a way as to obtain a well-defined error in the determined scaling coefficient. Consider several data points measured with increasing incident intensities. The integration time at each incident intensity is varied to control the error bar on each of the data points, such that the error bars on the log–log plot have equal width. This can be achieved by making the signal-noise-ratio (SNR) the same at every data point via the number of measurements at each data point. Let $\mu$ be the population mean, $\bar{x}$ be the sample mean, $\sigma^2$ be population variance, and $s^2$ be sample variance. With $n$ samples, we have $\mu = \bar{x} \pm t_{n-1}\frac{s}{\sqrt{n}} = \bar{x} \pm \Delta x$ for 95% confidence under t-distribution, and we define $SNR = K = \bar{x}/\Delta x$. Now $\bar{x}$ and $s$ can be obtained through measurements and the estimated number of samplings $n$ to reach the desired $SNR = K$ is $n = \left[\frac{K \cdot t_{n-1} s}{\bar{x}}\right]^2$. With these definitions, we developed the following procedure to reach a desired $SNR = K$:

1. Take $n_0$ = 10 measurements and calculate $\bar{x}_{10}$ and $s_{10}$. In our case we collect photon counts in 5 s segments for 10 times.
2. Compare $K_{10} = \bar{x}_{10}/t_{10-1}\frac{s_{10}}{\sqrt{10}}$ to the desired $SNR$, $K$, where $t_9$ = 2.262. If $K_{10} > K$, we conclude that the desired $SNR$ is reached and take $\bar{x}_{10}$ as the signal count rate.
3. If $K_{10} < K$, we enlarge $n_1$ by $n_1 = \left[\frac{K \cdot t_{10-1} s_{10}}{\bar{x}_{10}}\right]^2$
4. Take additional $n_1 - n_0$ points. Calculate $\bar{x}_{n_1}$, $s_{n_1}$ and $K_{n_1}$. Note $\bar{x}_n$ and $s_n$ will converge as $n \to \infty$.
5. Repeat 2–4.



DOI: 10.1021/acsnano.7b01665
ACS Nano 2017, 11, 5925–5932

The procedure ensures that on each data point, the error bars on the log−log plot are with equal width log $\frac{K+1}{K-1}$, hence minimizing the variance of the extracted fitted linear slope on the log−log plot.

## AUTHOR INFORMATION


### Corresponding Author

*tnorris@umich.edu.

### ORCID

Miao-Bin Lien: 0000-0003-4370-0480

Nicholas A. Kotov: 0000-0002-6864-5804


### Notes

The authors declare no competing financial interest.

## ACKNOWLEDGMENTS

This work was supported by the National Science Foundation through NSF DMR 1120923. The work at Brookhaven National Laboratory was supported by the Materials Science and Engineering Divisions, Office of Basic Energy Sciences of the U.S. Department of Energy under contract no. DESC0012704. Electron holography experiments were carried out in part at the Center for Functional Nanomaterials, Brookhaven National Laboratory. The HAADF images and the CBED patterns were taken at NIST.

## REFERENCES


(1) Mohamed, M. B.; Volkov, V.; Link, S.; El-Sayed, M. A. The 'lightning' Gold Nanorods: Fluorescence Enhancement of over a Million Compared to the Gold Metal. *Chem. Phys. Lett.* **2000**, *317*, 517−523.

(2) Kauranen, M.; Zayats, A. V. Nonlinear Plasmonics. *Nat. Photonics* **2012**, *6*, 737−748.

(3) Link, S.; Mohamed, M. B.; El-Sayed, M. A. Simulation of the Optical Absorption Spectra of Gold Nanorods as a Function of Their Aspect Ratio and the Effect of the Medium Dielectric Constant. *J. Phys. Chem. B* **1999**, *103*, 3073−3077.

(4) Jain, P. K.; Lee, K. S.; El-Sayed, I. H.; El-Sayed, M. A. Calculated Absorption and Scattering Properties of Gold Nanoparticles of Different Size, Shape, and Composition: Applications in Biological Imaging and Biomedicine. *J. Phys. Chem. B* **2006**, *110*, 7238−7248.

(5) Ni, W.; Kou, X.; Yang, Z.; Wang, J. Tailoring Longitudinal Surface Plasmon Wavelengths, Scattering and Absorption Cross Sections of Gold Nanorods. *ACS Nano* **2008**, *2*, 677−686.

(6) Fava, D.; Nie, Z.; Winnik, M. A.; Kumacheva, E. Evolution of Self-Assembled Structures of Polymer-Terminated Gold Nanorods in Selective Solvents. *Adv. Mater.* **2008**, *20*, 4318−4322.

(7) York, J.; Spetzler, D.; Xiong, F.; Frasch, W. D. Single-Molecule Detection of DNA via Sequence-Specific Links between F1-ATPase Motors and Gold Nanorod Sensors. *Lab Chip* **2008**, *8*, 415−419.

(8) Wang, H.; Huff, T. B.; Zweifel, D. A.; He, W.; Low, P. S.; Wei, A.; Cheng, J.-X. In Vitro and in Vivo Two-Photon Luminescence Imaging of Single Gold Nanorods. *Proc. Natl. Acad. Sci. U. S. A.* **2005**, *102*, 15752−15756.

(9) Huang, X.; El-Sayed, I. H.; Qian, W.; El-Sayed, M. A. Cancer Cell Imaging and Photothermal Therapy in the near-Infrared Region by Using Gold Nanorods. *J. Am. Chem. Soc.* **2006**, *128*, 2115−2120.

(10) Durr, N. J.; Larson, T.; Smith, D. K.; Korgel, B. A.; Sokolov, K.; Ben-Yakar, A. Two-Photon Luminescence Imaging of Cancer Cells Using Molecularly Targeted Gold Nanorods. *Nano Lett.* **2007**, *7*, 941−945.

(11) Boyd, G. T.; Yu, Z. H.; Shen, Y. R. Photoinduced Luminescence from the Noble Metals and Its Enhancement on Roughened Surfaces. *Phys. Rev. B: Condens. Matter Mater. Phys.* **1986**, *33*, 7923−7936.

(12) Farrer, R. A.; Butterfield, F. L.; Chen, V. W.; Fourkas, J. T. Highly Efficient Multiphoton-Abrortion-Induced Luminescence from Gold Nanoparticles. *Nano Lett.* **2005**, *5*, 1139−1142.

(13) Tong, L.; Wei, Q.; Wei, A.; Cheng, J.-X. Gold Nanorods as Contrast Agents for Biological Imaging: Optical Properties, Surface Conjugation and Photothermal Effects. *Photochem. Photobiol.* **2009**, *85*, 21−32.

(14) Lippitz, M.; van Dijk, M. A.; Orrit, M. Third-Harmonic Generation from Single Gold Nanoparticles. *Nano Lett.* **2005**, *5*, 799−802.

(15) Schwartz, O.; Oron, D. Background-Free Third Harmonic Imaging of Gold Nanorods. *Nano Lett.* **2009**, *9*, 4093−4097.

(16) Singh, A.; Lehoux, A.; Remita, H.; Zyss, J.; Ledoux-Rak, I. Second Harmonic Response of Gold Nanorods: A Strong Enhancement with the Aspect Ratio. *J. Phys. Chem. Lett.* **2013**, *4*, 3958−3961.

(17) Dadap, J. I.; Shan, J.; Eisenthal, K. B.; Heinz, T. F. Second-Harmonic Rayleigh Scattering from a Sphere of Centrosymmetric Material. *Phys. Rev. Lett.* **1999**, *83*, 4045−4048.

(18) Dadap, J. I.; Shan, J.; Heinz, T. F. Theory of Optical Second-Harmonic Generation from a Sphere of Centrosymmetric Material: Small-Particle Limit. *J. Opt. Soc. Am. B* **2004**, *21*, 1328−1347.

(19) Hao, E. C.; Schatz, G. C.; Johnson, R. C.; Hupp, J. T. Hyper-Rayleigh Scattering from Silver Nanoparticles. *J. Chem. Phys.* **2002**, *117*, 5963−5966.

(20) Russier-Antoine, I.; Benichou, E.; Bachelier, G.; Jonin, C.; Brevet, P. F. Multipolar Contributions of the Second Harmonic Generation from Silver and Gold Nanoparticles. *J. Phys. Chem. C* **2007**, *111*, 9044−9048.

(21) Bachelier, G.; Russier-Antoine, I.; Benichou, E.; Jonin, C.; Brevet, P.-F. Multipolar Second-Harmonic Generation in Noble Metal Nanoparticles. *J. Opt. Soc. Am. B* **2008**, *25*, 955−960.

(22) Butet, J.; Duboisset, J.; Bachelier, G.; Russier-Antoine, I.; Benichou, E.; Jonin, C.; Brevet, P.-F. Optical Second Harmonic Generation of Single Metallic Nanoparticles Embedded in a Homogeneous Medium. *Nano Lett.* **2010**, *10*, 1717−1721.

(23) Hubert, C.; Billot, L.; Adam, P.-M.; Bachelot, R.; Royer, P.; Grand, J.; Gindre, D.; Dorkenoo, K. D.; Fort, A. Role of Surface Plasmon in Second Harmonic Generation from Gold Nanorods. *Appl. Phys. Lett.* **2007**, *90*, 181105.

(24) Beversluis, M. R.; Bouhelier, A.; Novotny, L. Continuum Generation from Single Gold Nanostructures through near-Field Mediated Intraband Transitions. *Phys. Rev. B: Condens. Matter Mater. Phys.* **2003**, *68*, 115433.

(25) Imura, K.; Nagahara, T.; Okamoto, H. Near-Field Two-Photon-Induced Photoluminescence from Single Gold Nanorods and Imaging of Plasmon Modes. *J. Phys. Chem. B* **2005**, *109*, 13214−13220.

(26) Bouhelier, A.; Bachelot, R.; Lerondel, G.; Kostcheev, S.; Royer, P.; Wiederrecht, G. P. Surface Plasmon Characteristics of Tunable Photoluminescence in Single Gold Nanorods. *Phys. Rev. Lett.* **2005**, *95*, 267405.

(27) Knittel, V.; Fischer, M. P.; de Roo, T.; Mecking, S.; Leitenstorfer, A.; Brida, D. Nonlinear Photoluminescence Spectrum of Single Gold Nanostructures. *ACS Nano* **2015**, *9*, 894−900.

(28) Panasyuk, G. Y.; Schotland, J. C.; Markel, V. A. Classical Theory of Optical Nonlinearity in Conducting Nanoparticles. *Phys. Rev. Lett.* **2008**, *100*, 47402.

(29) Nikoobakht, B.; El-Sayed, M. A. Preparation and Growth Mechanism of Gold Nanorods (NRs) Using Seed - Mediated Growth Method. *Chem. Mater.* **2003**, *15*, 1957−1962.

(30) Kim, J.-Y.; Lien, M.-B.; Han, M.-G.; Zhu, Y.; Norris, T.; Kotov, N. Charge Anisotropy of Gold Nanorods. *251st American Chemical Society National meeting & Exposition*; American Chemical Society: San Diego, 2016; p 244.

(31) Völkl, E.; Allard, L. F.; Joy, D. C. *Introduction to Electron Holography*; 1st ed.; Springer: US, 1999; Vol. *53*.

(32) Kim, J.-Y.; Lien, M.-B.; Han, M.-G.; Magonov, S.; Zhu, Y.; Ferguson, H.; Norris, T.; Kotov, N. Hidden Electrostatic Asymmetry of Gold Nanorods. *Sci. Adv.* **2017**, submitted.

(33) Boyd, R. W. *Nonlinear Optics*, 3rd ed.; Academic Press, 2008.

(34) Groeneveld, R. H. M.; Sprik, R.; Lagendijk, A. Femtosecond Spectroscopy of Electron-Electron and Electron-Phonon Energy




DOI: 10.1021/acsnano.7b01665
*ACS Nano* 2017, 11, 5925−5932

Relaxation in Ag and Au. *Phys. Rev. B: Condens. Matter Mater. Phys.* **1995**, *51*, 11433−11445.
(35) Perner, M.; Bost, P.; Lemmer, U.; von Plessen, G.; Feldmann, J.; Becker, U.; Mennig, M.; Schmitt, M.; Schmidt, H. Optically Induced Damping of the Surface Plasmon Resonance in Gold Colloids. *Phys. Rev. Lett.* **1997**, *78*, 2192−2195.
(36) Lin, Z.; Zhigilei, L. V.; Celli, V. Electron-Phonon Coupling and Electron Heat Capacity of Metals under Conditions of Strong Electron-Phonon Nonequilibrium. *Phys. Rev. B: Condens. Matter Mater. Phys.* **2008**, *77*, 75133.
(37) Verellen, N.; Denkova, D.; Clercq, B.; Silhanek, A. V.; Ameloot, M.; Dorpe, P.; Moshchalkov, V. V. Two-Photon Luminescence of Gold Nanorods Mediated by Higher Order Plasmon Modes. *ACS Photonics* **2015**, *2*, 410−416.
(38) Mertens, J.; Kleemann, M.-E.; Chikkaraddy, R.; Narang, P.; Baumberg, J. J. How Light Is Emitted by Plasmonic Metals. *Nano Lett.* **2017**, *17*, 2568−2574.
(39) Hayes, W.; Loudon, R. *Scattering of Light by Crystals*; John Wiley & Sons, 1978; Ch 1.
(40) Agarwal, G. S. Brownian Motion of a Quantum Oscillator. *Phys. Rev. A: At., Mol., Opt. Phys.* **1971**, *4*, 739−747.
(41) Agarwal, G. S. Quantum Electrodynamics in the Presence of Dielectrics and Conductors. I. Electromagnetic-Field Response Functions and Black-Body Fluctuations in Finite Geometries. *Phys. Rev. A: At., Mol., Opt. Phys.* **1975**, *11*, 230−242.
(42) Link, S.; El-Sayed, M. A. Spectroscopic Determination of the Melting Energy of a Gold Nanorod. *J. Chem. Phys.* **2001**, *114*, 2362−2368.



DOI: 10.1021/acsnano.7b01665
*ACS Nano* 2017, 11, 5925−5932